



# Ocean–atmosphere processes associated with enhanced Indian monsoon break spells in CFSv2 forecasts

Balachandrudu Narapusetty<sup>1,2,5</sup> · Raghu Murtugudde<sup>3</sup> · Hui Wang<sup>4</sup> · Arun Kumar<sup>4</sup>

Received: 5 June 2017 / Accepted: 1 December 2017  
© Springer-Verlag GmbH Germany, part of Springer Nature 2017

## Abstract

This paper analyzes the role of ocean–atmosphere processes associated with break days and their impact on dry-land biases of Indian summer monsoon in Climate Forecast System version 2 (CFSv2)’s sub daily and monthly hindcasts, which are produced by initializing the forecast system every 5 days in each month from January 1982 to December 2007. Each initialized forecast produces 24 ensemble members and they are characterized by a systematic dry-land bias over central India and have been interlinked with higher break days in majority of the ensemble members. Analyses on 15–45 day band-passed summer precipitation anomalies indicate that the monsoon intraseasonal oscillations are very weak in Mar- and Apr-initialized forecasts while they get stronger in May- and Jun-initialized forecasts. The persistent low-level anticyclonic activity in the Findlater jet in the longer lead months (Mar- and Apr-initialized forecasts) is systematically diminished in the summer forecasts that are produced by initializing the forecast system closer to the June–September (JJAS) season (e.g., May- and Jun-initialized forecasts). This low-level negative vorticity bias extends across central India and diminishes with the systematic oceanic mixed layer shoaling in the northern Bay of Bengal (BoB) and Indian Ocean (IO). The deeper ocean mixed layer in BoB and northern IO in conjunction with persistent negative vorticity biases suppresses intraseasonal variability of Indian summer monsoon rainfall and induces a large number of break days, which lead to the dry-land biases in July and August in the core monsoon zone. CFSv2-produced Pacific sea surface temperatures exert a strong influence on mixed layer depths (MLDs) across the basins in Arabian Sea (AS), BOB and IO unlike in observations. The forecasted extended break spells are systematically and highly correlated with the model produced Niño3 index while no such strong correlation is found between total monsoonal break days and ENSO in the observations. The May- and Jun-initialized CFSv2 forecasts reproduce the Indian summer monsoon rainfall in July–August reliably by reasonably alleviating the ocean–atmosphere coupled biases relative to earlier initializations.

**Keywords** CFSv2 sub daily forecasts · Extended break events · Indian Summer Monsoon dry-land biases · Systematic delay in monsoon onset

## 1 Introduction

The Indian Summer Monsoon Rainfall (ISMR) accounts for more than 75% of total annual rainfall over India and is regarded as lifeline for over a billion people by significantly affecting agriculture, water resources, hydropower generation and numerous other socio-economic sectors. The ISMR directly impacts the Kharif crop season, which runs from June to October and provides more than 50% of the total food grain production. Since 2015, the India Meteorological Department (IMD) has started issuing the much needed ISMR forecasts based on dynamical forecasting efforts (Borah et al. 2013; Abhilash et al. 2014) as the current generation coupled general circulation models

✉ Balachandrudu Narapusetty  
bala.narapusetty@noaa.gov

<sup>1</sup> INNOVIM and NOAA/NWS/NCEP/Climate Prediction Center, College Park, MD, USA

<sup>2</sup> Earth System Science Interdisciplinary Center, College Park, MD, USA

<sup>3</sup> Department of Atmospheric and Oceanic Science, Earth System Science Interdisciplinary Center, University of Maryland, College Park, MD, USA

<sup>4</sup> NOAA/NWS/NCEP/Climate Prediction Center, College Park, MD, USA

<sup>5</sup> NOAA Center for Weather and Climate Prediction, 5830 University Research Court, College Park, MD 20740, USA

(CGCMs) can effectively represent interactions among land, atmosphere and ocean and include latest data assimilation schemes in initializing forecast systems. These CGCMs have shown to produce seasonal forecasts with more realistic ISMR variability compared to the empirical models, which are commonly used in providing ISMR seasonal forecasts (DelSole and Shukla 2012; Borah et al. 2013; Abhilash et al. 2014).

The CGCM forecast systems, however, are well known for their systematic biases in reproducing ISMR on seasonal scale. Process-based understanding of the seasonal evolution of ISMR biases in the Coupled Model Intercomparison Project Phase 3 (CMIP3) and CMIP5 models have been extensively reported to highlight the large-scale ocean–atmosphere biases (Lee et al. 2010; Sperber et al. 2013; Ashfaq et al. 2016). The intraseasonal variabilities (ISVs) in CMIP5 CGCMs have also been extensively studied as the precipitation corresponding to the ISVs of June–September rainfall is a major part of the total precipitation variability over Indian subcontinent (Krishnamurthy and Shukla 2000, 2008; Annamalai and Slingo 2001; Zhou et al. 2016). In this study, we explore the systematic biases in intraseasonal precipitation and the associated ocean and atmosphere seasonal variations produced by daily and monthly forecasts of Climate Forecast System version 2 (CFSv2; Saha et al. 2014). The CFSv2 seasonal forecasts which are routinely produced for use in operational products have been extensively studied for the representation and improvements of seasonal forecasting capability of ISMR (Jiang et al. 2013; Pokhrel et al. 2013, 2016; Narapusetty et al. 2015). The CFSv2 also produces sub-daily forecasts and the intraseasonal variability produced by the CFSv2 sub-seasonal forecasts has been a topic of active research given the importance of reliably forecasting the active and break spells of ISMR (Sahai et al. 2013; Abhilash et al. 2014; Goswami et al. 2014; Krishnamurthy 2017). Our analysis presented here advance the process understanding these biases and highlights the role of the ocean in amplifying the coupled climate forecasts.

The seasonal evolution of ISMR biases in CFSv1 and CFSv2 simulations and forecasts is well documented along with the indication of delayed onset of the summer monsoon (Achuthavarier and Krishnamurthy 2010; Lee Drbohlav and Krishnamurthy 2010; Chaudhari et al. 2012; Goswami et al. 2014; Narapusetty et al. 2015). The typical northward migration of the Intertropical Convergence Zone (ITCZ) in April, which impacts the onset of the monsoon, is shown to be delayed in the CFSv2 monthly forecasts (Narapusetty et al. 2015) and acts to trigger the dry-land biases in conjunction with systematic bias in low-level wind and sea surface temperatures (SSTs). Weaker ISVs in CFSv2 daily forecasts are also well correlated with enhanced mixed layer depth (MLD) in Indian Ocean which is consistent with the weakening of the northward moving monsoon intraseasonal

oscillations (MISOs) originating in the northern Equatorial Indian Ocean (Roxy et al. 2013).

A prominent feature of ISMR is the occurrence of active and break episodes, which strongly influences the ISVs (Sikka and Gadgil 1980; Krishnamurti and Ardanuy 1980; Goswami and Ajaymohan, 2001; Rajeevan et al. 2010). While the frequency and the intensity of the active and break spells directly impact the excess and deficit of the average ISMR (Gadgil and Joseph 2003), prolonged break days are shown to induce stress on the agriculture production in the Kharif season (Gadgil and Rupa Kumar 2006; Krishna Kumar et al. 2004; Prasanna 2014).

Given the need for understanding of systematic dry-land biases in the CGCMs, the break episodes of ISMR (that can result in continental dryness) provide a possible linkage between large-scale ocean–atmosphere coupled biases and the dry-land biases over India. To this end, the primary objective of this study is to understand the role of break spells, which are associated with ocean–atmosphere processes, on the systematic dry-land biases in ISMR using CFSv2 produced sub daily and monthly forecasts from January 1982 to December 2007. The manuscript is organized as follows: the observational datasets and the CFSv2 hindcasts used in this study are described in Sect. 2; analysis and results are presented and discussed in Sect. 3 and the conclusions and future work are summarized in Sect. 4.

## 2 Description of the forecast system and observational datasets

Daily and monthly-mean seasonal forecasts used in this study are obtained from CFSv2 retrospective forecasts (Saha et al. 2014). Sub-daily forecasts of precipitation and zonal wind at 850 hPa available at 6 h frequency are aggregated to daily time-scale and used along with monthly forecasts of SST, MLDs, zonal and meridional winds at 850 hPa and zonal wind at 10 m. The forecasts are initialized each month from January 1982 to March 2011 to produce 9 month-lead forecasts; however, the sub-daily data is only available till December 2009. The CFSv2 system produces 24 ensemble member forecasts for each month, except when initialized in the month of November, which generates 28 members. The atmospheric component of CFSv2 is the NCEP Global Forecast System (GFS) at 0.938° spatial resolution and the ocean component is the Geophysical Fluid Dynamics Laboratory (GFDL) Modular Ocean Model version 4 (MOM4) that has a spatial resolution in the zonal direction of 0.5°. In the meridional direction the resolution is 0.25° from 10°S to 10°N, progressively decreasing to 0.5° from 10° to 30°, and is fixed at 0.5° beyond 30° in both hemispheres. In the coupled framework of CFSv2, the atmosphere and the ocean components exchange freshwater, heat, and momentum

fluxes every 30 min during the forecast. For observations, this study uses APHRODITE precipitation, which is available from 1961 to 2007 (Yatagai et al. 2012) and CFS reanalysis product (CFSR; Saha et al. 2010) for coherent ocean and 3-D atmospheric data. The daily and the monthly mean values of precipitation, ocean MLDs and zonal and meridional winds at 850 hPa are also obtained from CFSR to estimate forecast biases and perform other analyses. We have also performed the analysis with MERRA2 reanalysis data and found that the conclusions are not affected by the choice of reanalysis product. Throughout this paper, a common timeframe of 1982–2007 is chosen for the analysis due to the data availability, and bias is calculated as the difference between CFSv2 forecasts and corresponding observations or reanalysis product. The analyses on CFSv2 forecasts that are presented in Sect. 3 are performed using ensemble mean state unless specified otherwise.

### 3 Results and discussion

#### 3.1 Spatial fidelity of ISMR distribution in the monsoon core region as produced by forecasts

The gridded correlation of daily precipitation in the core monsoon zone during July and August of 1982–2007 with rest of India is shown in Fig. 1 for observations and Mar- to Jun-initialized ensemble mean forecasts. The core monsoon zone is shown with a polygon in each of the subplots of Fig. 1 and is selected to avoid the Himalayan foothills as described by Rajeevan et al. (2010: referred to as R2010 hereafter).

Figure 1a shows the correlation using APHRODITE precipitation data. The key features such as negative correlation at foothills and southeast peninsular India match very closely with R2010's analysis, which was produced using gauge data of IMD from 1951 to 2007. The correlations depicted in Mar- to Jun-initialized July–August forecasts (Fig. 1b–e) reproduce the key observed features but fail to capture the severity and extension of negative correlation in the foothills and southeast peninsula and positive correlation along the Western Ghats in Mar- and Apr-initialized forecasts. In the forecasts, the stronger positive correlation is mainly concentrated to the west of the highest positively correlated area in the observations and fails to replicate the northwest–southeast tilt (Fig. 1b, c). In the May-initialized forecasts, the northwest-southeast tilt in the core monsoon zone, and positive correlations in Western Ghats are better reproduced than in the Mar- and Apr-initialized forecasts with a strong indication of negative correlation over the southeast peninsular India (Fig. 1d).

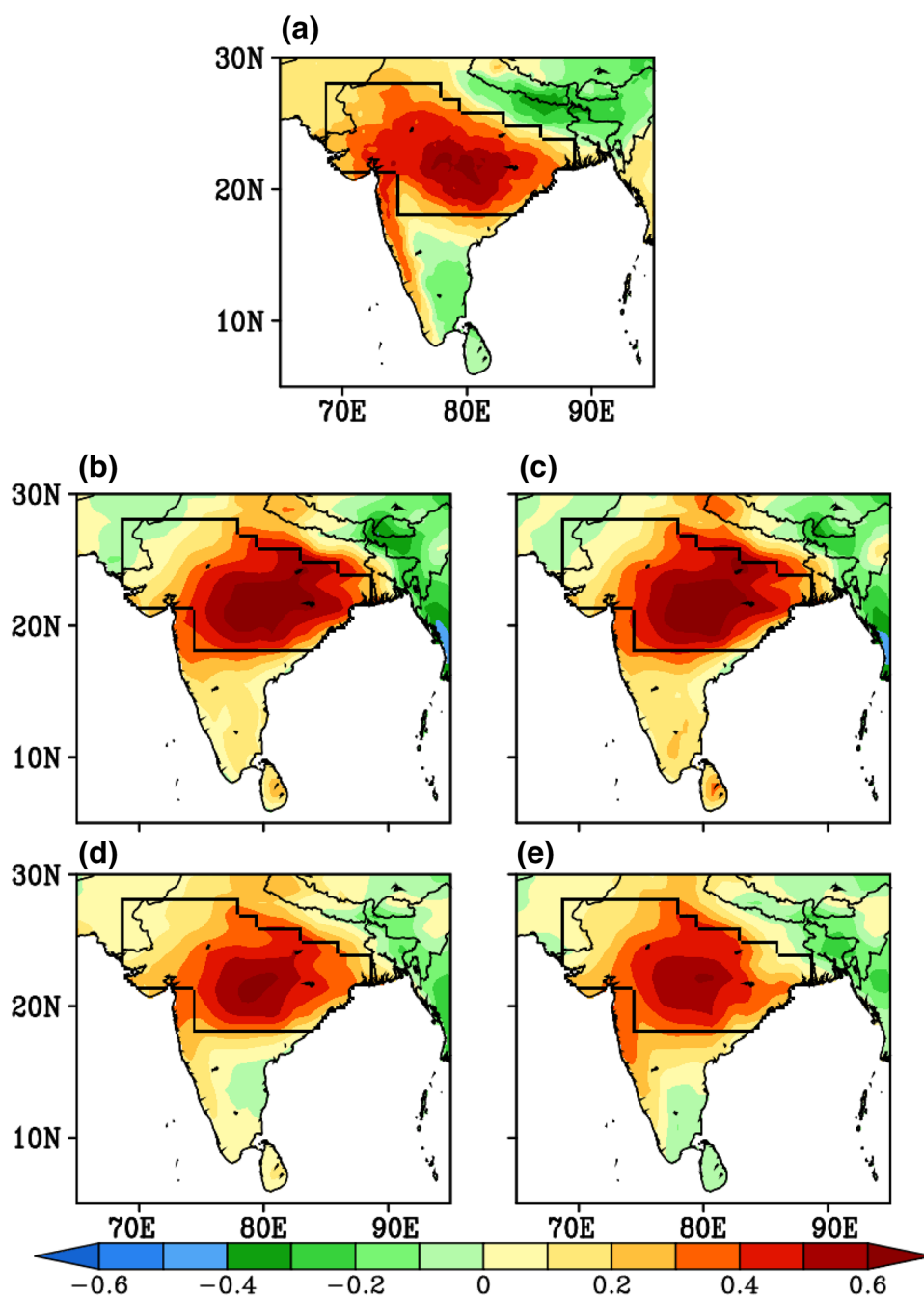
Compared to the Mar- to May-initialized forecasts, the Jun-initialized forecasts well replicate negative correlations over the southeast peninsula, much stronger correlation with precipitation in the Western Ghats along with the northwest–southeast tilt of positive correlations in the core monsoon zone (Fig. 1e). The negative correlation that is a key feature in observations (Fig. 1a) has systematically shifted to northeastward. The systematic negative correlation to the northeast of the core monsoon zone as produced by the Mar- to May-initialized forecasts is reduced in the Jun-initialized forecasts albeit the extent and severity of negative correlation in the Himalayan foothills is not well reproduced.

#### 3.2 Analysis of break days

The ensemble mean of July–August CFSv2 forecasts initialized in the months of March to June show systematically higher number of break days than in the APHRODITE product (Fig. 2). An earlier pioneering study by Ramamurthy (1969) identified the break spells based upon the persistent monsoonal trough over Himalayan foothills for at least two consecutive days. In this study, the number of break days in each year is estimated as the days having negative rainfall anomaly for at least three consecutive days below one standard deviation (similar to R2010). Throughout the analysis the daily anomalies are estimated by removing the climatological mean as described by Narapusetty et al. (2009). The years with higher number of break days in APHRODITE data closely match with the R2010's analysis based on July–August rainfall in the years 1951–2007; for example the high number of break days in the years 1987, 1993, 2002 and 2005, respectively, closely match with the R2010's analysis using IMD precipitation data (Fig. 6b of R2010). CFSv2 forecasts produce a wide variation in the number of break days up to 34 days across the years while the break days in observations maximize at 20. The forecasts show high numbers of break days in a year when the observations show relatively fewer break days. In majority of the years, the Mar-initialized forecasts show higher and Jun-initialized forecasts show fewer break days (depicted by blue and red symbols in Fig. 2).

The frequency distribution of break days at various periods shows that the forecasts produce more high (3–6 days) and low frequency (> 10 days) break spells (Table 1). The discrepancy in the lowest duration of break spells (3–4 days) between the observations and forecasts is well expected and easily understood from persistent anticyclonic biases in forecasts over the core monsoon zone (Narapusetty et al. 2015). Longer break spells are especially higher in Apr- and May-initialized forecasts while JUN-initialized forecasts show no break event with durations beyond 10 days compared to the earlier initialized forecasts. The mean and standard deviation of break

**Fig. 1** Gridded correlation of the core monsoon zone (shown in polygon in all the plots) with the entire subcontinent in July–August of 1982–2007 in **a** APHRODITE data, and CFSv2 forecasted July–August by initializing in the beginning of **b** March, **c** April, **d** May, and **e** June



days in July–August of 1982–2007 are 6.2 and 5.5 days from APHRODITE data. The May- and Jun-initialized CFSv2 forecasts show comparable days of average break events, while all the CFSv2 forecasts show larger standard deviation (Table 2). The mean and the standard deviation gradually decrease from Mar- to Jun-initialized forecasts except the Apr-initialized forecasts, which show higher mean and variations than the March initialized forecasts. This is reminiscent of the higher skill of some longer lead forecasts compared to the shorter lead forecasts (Chattopadhyay et al. 2015).

The systematically higher break spells produced by ensemble mean forecasts can be traced back to majority of the individual ensemble members forecasting longer break spells. The probability among the 24 ensemble members to reproduce total break days longer than 15 days in each of March to June forecasted July–August months is shown in Fig. 3. The X-axis shows the number of ensemble members that agree with the event of producing higher than 15 break days in the July–August forecasts. In general the concurrent observations show much lower than 15 break days (as shown on Y-axis) while most

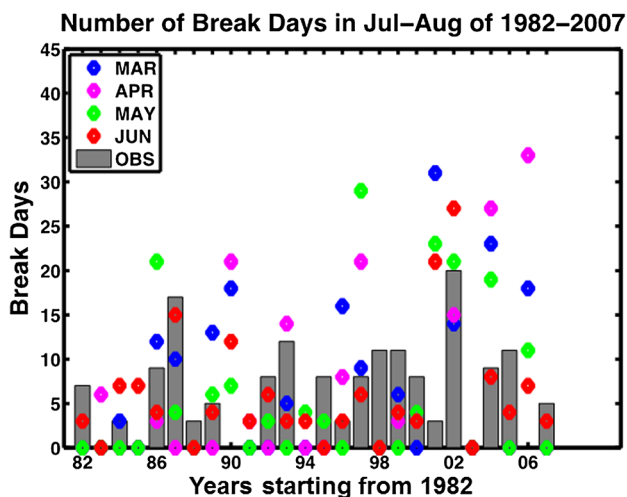


**Fig. 2** Total number of break days in July and August of 1982–2007 using the APHRODITE precipitation product as shown in grey bars, March- to June-initialized CFSv2 forecasts for the same months in blue, magenta, green and red diamond symbols

of the Mar- to Jun-initialized ensemble forecasts produce higher than 15 days of break during July and August months. In particular, of all the available ensemble combinations, the Mar-initialized forecast ensembles generally produce higher than 15 break days (red line in Fig. 3) while the concurrent observations show a much lower number of break days. APR- to Jun-initialized forecasts show that when observations are closer to break periods of 15 days, more than 9 ensemble members forecast more than 15 break days. While MAR-, May- and Jun-initialized forecast ensembles show a systematic tendency to generate longer break periods, Apr-initialized forecast ensembles do not show such a consistency (green line in Fig. 3), although most of the ensemble members show more than the observed break days. The inconsistency of Apr-initialized ensemble forecasts show a larger disagreement among the ensemble members indicating a higher ensemble spread. Indeed, the Apr-initialized forecasts show marginally higher ensemble spread for July–August forecasted precipitation for several years compared to the

**Table 2** Mean and standard deviation of break events in July–August of 1982–2007

Dataset	Mean (in days)	Standard deviation (in days)
APHRODITE	6.2	5.5
Monthly initialized CFSv2 forecasts		
March	6.9	8.8
April	8.3	13.9
May	6.0	8.9
June	5.9	6.5

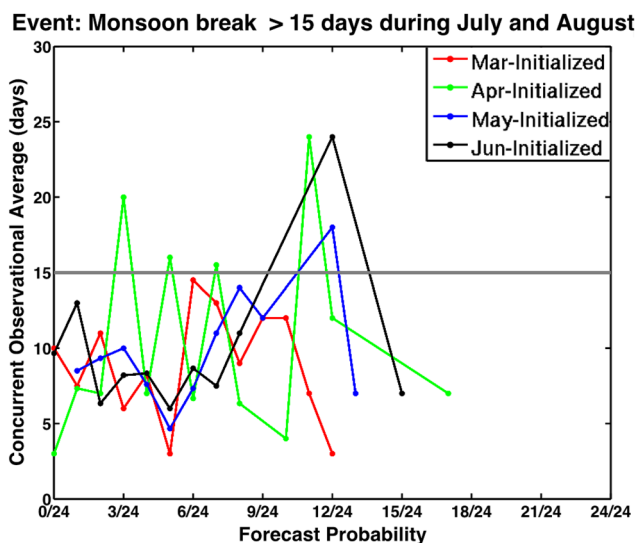


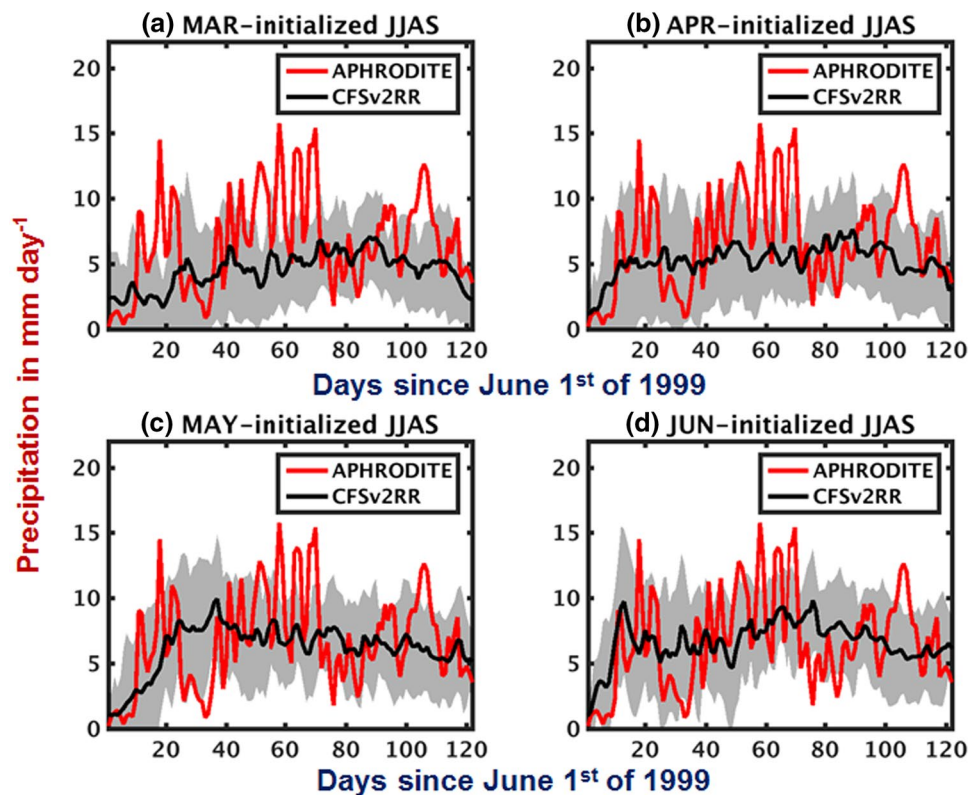
**Fig. 3** Probability of March- to June-initialized forecast ensembles agreeing on having monsoon break events longer than 15 days during July–August of 1982–2007 shown on the X-axis and the concurrent observation averages are shown on the Y-axis

other initialized months (grey shading in Fig. 4b shown for the year 1999). Higher initial error can be expected to grow into larger biases over longer lead times.

**Table 1** Frequency distribution of break spells as a percentage of the total number of break days

Duration (days)	APHRODITE	March-initial-ized	April-initial-ized	May-initial-ized	Jun-initial-ized
3–4	43	70	57	67	62
5–6	23	18	10	13	26
7–8	23	5	10	3	9
9–10	10	3	10	7	3
11–12	0	5	7	7	0
13–14	0	0	3	3	0
> 15	0	0	3	0	0

**Fig. 4** CFSv2 forecasted ensemble mean daily precipitation (Y-axis: in  $\text{mm day}^{-1}$ ) averaged over central India ( $16^{\circ}$ – $26.5^{\circ}\text{N}$ ;  $74^{\circ}$ – $87^{\circ}\text{E}$ ) for JJAS (X-axis) in 1999 initialized at the beginning of **a** March, **b** April, **c** May and **d** June. In all the subplots the gray shading shows the ensemble spread



### 3.3 Intraseasonal variability in CFS forecasts

The daily mean precipitation produced by CFS forecasts is systematically lower than observations in any year. As an example, Fig. 4 shows the ensemble mean and spread of daily precipitation averaged over central India ( $16^{\circ}$ – $26.5^{\circ}\text{N}$ ;  $74^{\circ}$ – $87^{\circ}\text{E}$ ) for JJAS as produced by Mar- to Jun-initialized forecasts for 1999. On average the MAR- and APR-initialized ensemble mean forecasts produce precipitation below  $5 \text{ mm day}^{-1}$ , which is much lower than the observations. The May- and Jun-initialized forecasts exhibit more realistic precipitation, however, in all the forecasts the amplitude of intraseasonal variability is much smaller compared to APHRODITE, partially due to the ensemble average. The Mar- to May-initialized forecasts severely underestimate the precipitation at the beginning of the summer mainly due to a systematic delay in the monsoon onset, which is confirmed with monsoon index as proposed by Wang et al. (2009; not shown).

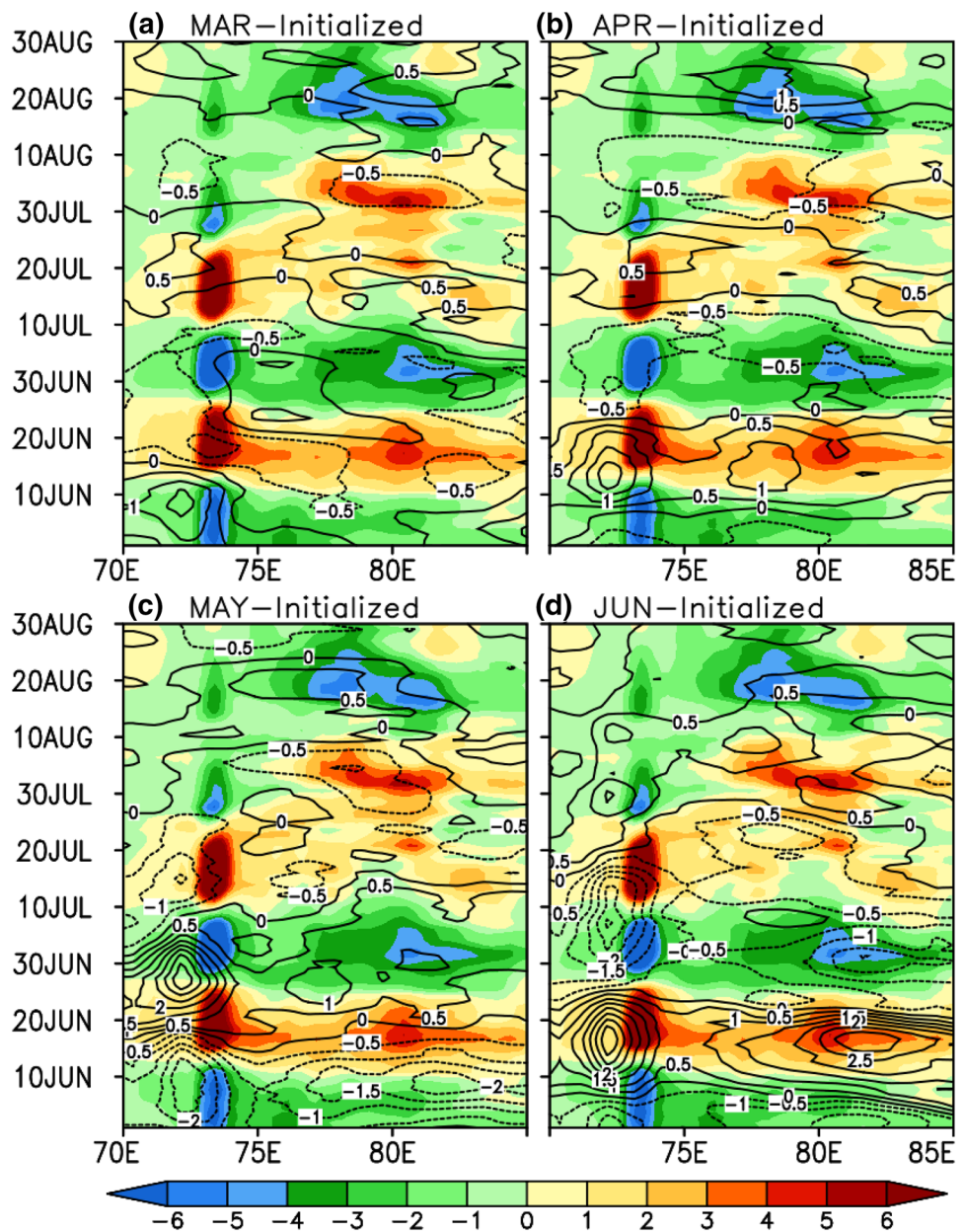
The MISOs are examined by producing the 15–45 day anomalies in the CFSv2 forecasts by band-passing the precipitation data for JJA in all the years (see Fig. 5). A Hovmöller diagram constructed over central India ( $16^{\circ}$ – $26.5^{\circ}\text{N}$ ) depicted for longitudes  $70^{\circ}$ – $85^{\circ}\text{E}$  shows much stronger MISOs with a slight northwest-southeast tendency (color shading in all the subplots of Fig. 5) in the observations. Intraseasonal variability is much weaker in the

MAR- and APR-initialized forecasts with a clear hint of slower propagation of MISOs (the contours in Fig. 5a, b lag behind the color shading) with no sign of a northwest tilt of the anomalies. The May-initialized forecasts show improvement in the strength of MISOs compared to the Mar- and Apr-initialized forecasts the Jun-initialized forecasts show further improvement in ISVs compared to observed variability (Fig. 5d). Figures 4 and 5 reveal that the CFSv2 forecasts systematically improve the total and intraseasonal variability when initialized closer to JJAS.

### 3.4 Ocean–atmosphere processes and intraseasonal variability

Several studies show that the local net flux heating, vertical diffusive mixing, Madden Julian oscillations, Findlater jet variations and salinity stratification control the MLDs in the IO, AS and BoB (Waliser et al. 2003, 2004; Vinayachandran et al. 2012; Drushka et al. 2012, 2014; Li et al. 2016, 2017). While Pacific ocean variability has shown to have little impact on the MLDs (Keerthi et al. 2013), there has been a discernible relationship between ENSO and intraseasonal variability over the IO, BOB and AS (Feng et al. 2015; Chen et al. 2016; Liu et al. 2016; Wu and Cao 2017; Zhou et al. 2017). Figure 6 shows the biases in the MLDs and low-level winds at 850 hPa for July–August of 1982–2007 produced by CFSv2 forecasts for various initialized months.

**Fig. 5** Contours show 15–45 day band-passed anomalies of CFSv2 forecasted ensemble mean daily precipitation (in  $\text{mm day}^{-1}$ ) averaged over latitudes  $16^{\circ}$ – $26.5^{\circ}\text{N}$  for June to August in 1999 produced by initializing at the beginning of **a** March, **b** April, **c** May and **d** June. In all the subplots the color shading represents the same precipitation anomalies using APHRODITE product for the same time

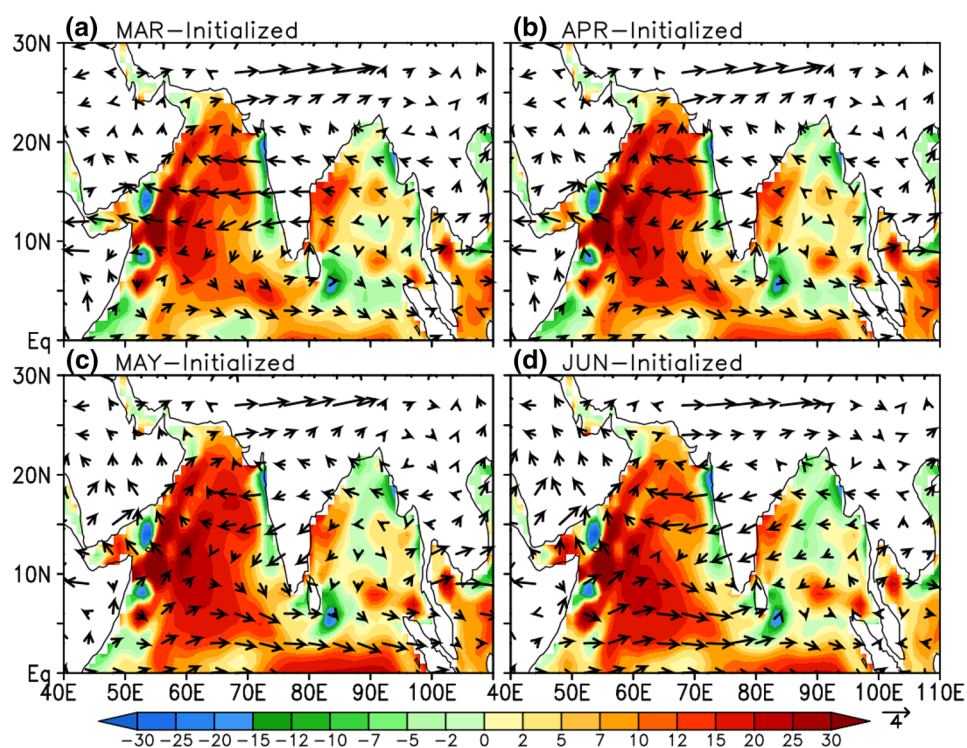


All CFSv2 forecasts show strong positive MLD biases in the equatorial IO (EIO), AS, and BoB.

However, as the initialized month for forecast gets closer to JJA, the biases become smaller in the key regions, where the major influences on the intraseasonal variability in the precipitation originate from (Sikka and Gadgil 1980; Krishnamurti and Ardanuy 1980; Yasunari 1980, 1981; Goswami and Ajaymohan 2001; Krishnamurthy 2016). For instance, the MLD biases in Mar- to Jun-initialized forecasts for July–August systematically decrease in the EIO ( $2^{\circ}$ – $10^{\circ}\text{N}$ ;  $70^{\circ}$ – $85^{\circ}\text{E}$ ) and northern BoB ( $14^{\circ}$ – $18^{\circ}\text{N}$ ;  $86^{\circ}$ – $92^{\circ}\text{E}$ ) and in the AS off the Kerala coast. The interannual time series of MLDs in the EIO and BoB from CFSR and the CFSv2 forecasts reveal that the MLDs reduce

systematically from Mar- to Jun-initialized July–August forecasts (not shown). The deepening of mixed layer in the EIO has been shown to suppress the MISOs (Roxy et al. 2013) while the precipitation in the northern BoB is shown to positively correlate with precipitation over central India (Meehl et al. 2012). Role of the ocean in intraseasonal precipitation is also shown to be dominant off the west coast of India (Xi et al. 2015). CFSv2 forecasts also show negative vorticity biases in the Findlater jet in the northern AS. MAR-initialized forecasts show stronger negative vorticity biases that stretch from AS to northern India and positive biases over southern tip of India (Fig. 6a). This negative vorticity is reduced over India in Apr- to Jun-initialized forecasts along with increased positive vorticity over the Western Ghats (not

**Fig. 6** Biases in mixed layer depths (m) in colors and 850 hPa winds ( $\text{m s}^{-1}$ ) as arrows for averaged July–August forecasts as reproduced in CFSv2 obtained by initializing at the beginning of **a** March, **b** April, **c** May and **d** June months

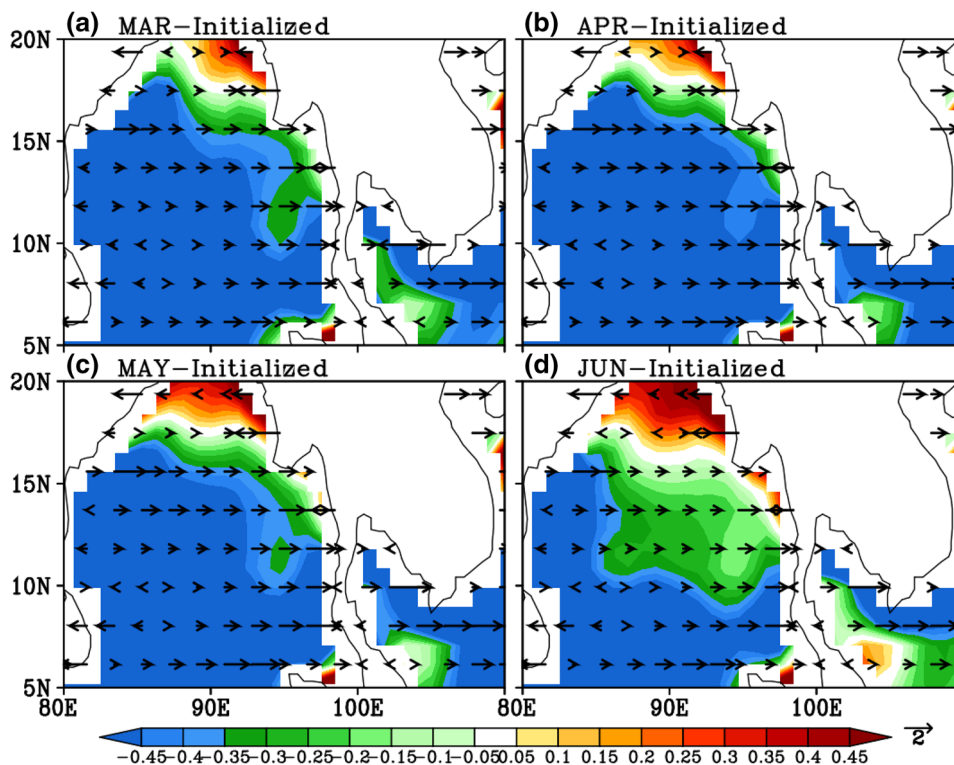


shown). The forecast biases at intraseasonal timescales are consistent with these vorticity biases (Goswami and Xavier 2005) and may be related to the coupled biases in the so-called Central Indian Ocean mode that is recently proposed

(Zhou et al. 2016). But this needs further analysis which is beyond the scope of the present study.

Figure 7 shows the biases in SSTs and 10 m zonal winds for July–August of 1982–2007 as produced by CFSv2

**Fig. 7** Biases in SST (colors) and 10-m zonal winds ( $\text{m s}^{-1}$ ) for July–August as reproduced in CFSv2 seasonal forecasts obtained by initializing the model at the beginning of **a** March, **b** April, **c** May and **d** June months





forecasts by initializing the model from March to June. The CFSv2 July–August forecasts are marked by negative SST biases over the EIO, AS and BoB. The negative SST biases decrease over BoB from MAR- to JUN-initialized forecasts albeit the SST biases are not reduced in the EIO (not shown). The SST and MLD biases are very coherent and reduce systematically from MAR- to JUN-initialized forecasts. In the head Bay as well as central BoB (85°–95°E and 5°–25°N), the general tendency is that the positive SST bias is strongly correlated with negative MLD biases. The CFSv2 forecasts are marked with stronger negative SST biases and positive MLD biases as the model is initialized farther from the summer season (e.g., March). In the head Bay region (above 20°N), the increase in the positive SST bias is correlated with a negative MLD bias and the spatial correlation reaches  $-0.54$  in Jun-initialized forecasts. This relation is also pronounced in 5°–20°N, where the SST bias systematically positive from Mar- to Jun-initialized forecasts and the MLD biases are reduced with spatial correlation reaching up to  $-0.7$ . The negative correlation between the SST and MLD biases in the BoB suggests to be driven, in part by the wind biases (Fig. 6).

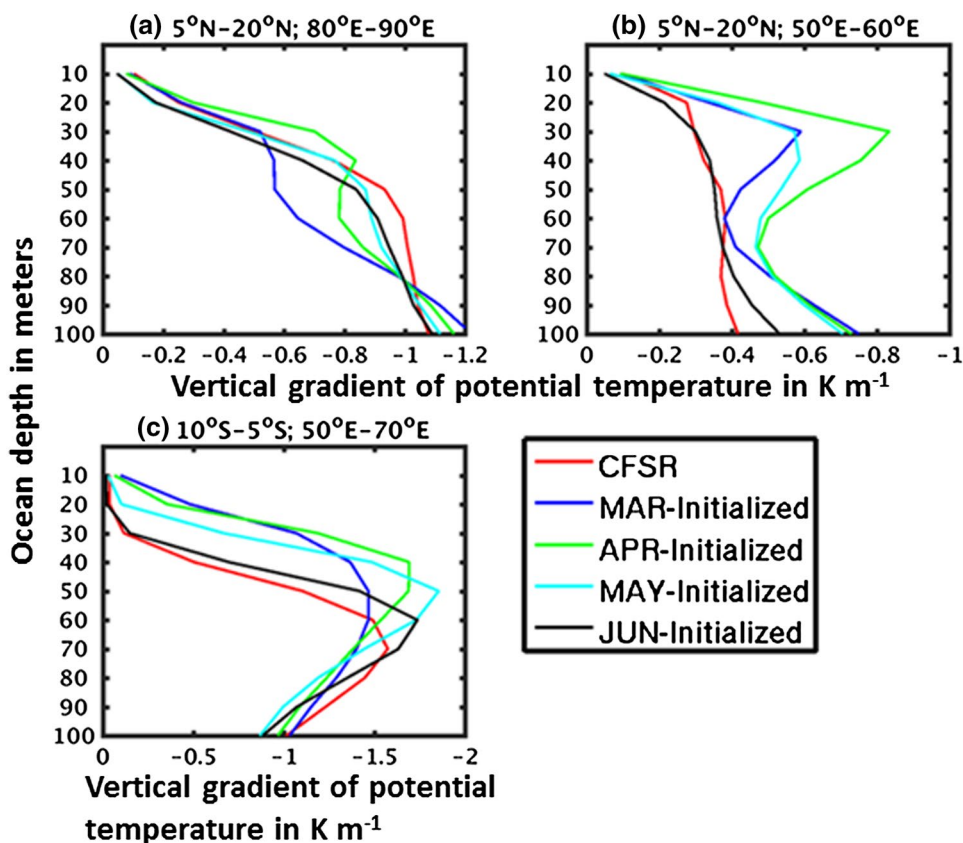
Figure 8 shows the vertical gradient of potential temperatures  $\left[\frac{\partial\theta}{\partial z}\right]$  as produced by CFSv2 forecasts and CFSR down to 100 m in BoB, AS and IO basins. The Mar- to

May-initialized forecasts exhibit systematic stratification biases; whereas the Jun-initialized forecasts are very similar to the vertical gradients produced by CFSR in all the basins. The evolution of vertical temperature gradients produced by the forecasts differs with CFSR data more strongly in BoB and AS regions and marginally in the southern IO basin. The stratification biases in BoB are coherent with the enhanced Rossby wave dynamics in July and August forecasts produced as a result of wind biases originating in the West Equatorial IO in the CFSv2 forecasts (Narapusetty et al. 2015) and the likely deficiencies in capturing the temperature inversions and the barrier layer structure in this fresh-water-forcing-dominated basin (Howden and Murtugudde 2001).

### 3.5 ENSO remote teleconnections

Majority of the studies have concentrated on the relation between ENSO and IOD, which peaks in the boreal fall, while the interannual variability of coupled ocean–atmospheric fluxes and the IO SSTs during summer are in part controlled by ENSO through the atmospheric bridge (Klein et al. 1999; Alexander et al. 2002; Lau and Nath 2000, 2003). The MLD in IO is partly controlled by atmospheric bridge-induced local radiative and evaporative flux feedbacks (Murtugudde and Busalacchi 1999;

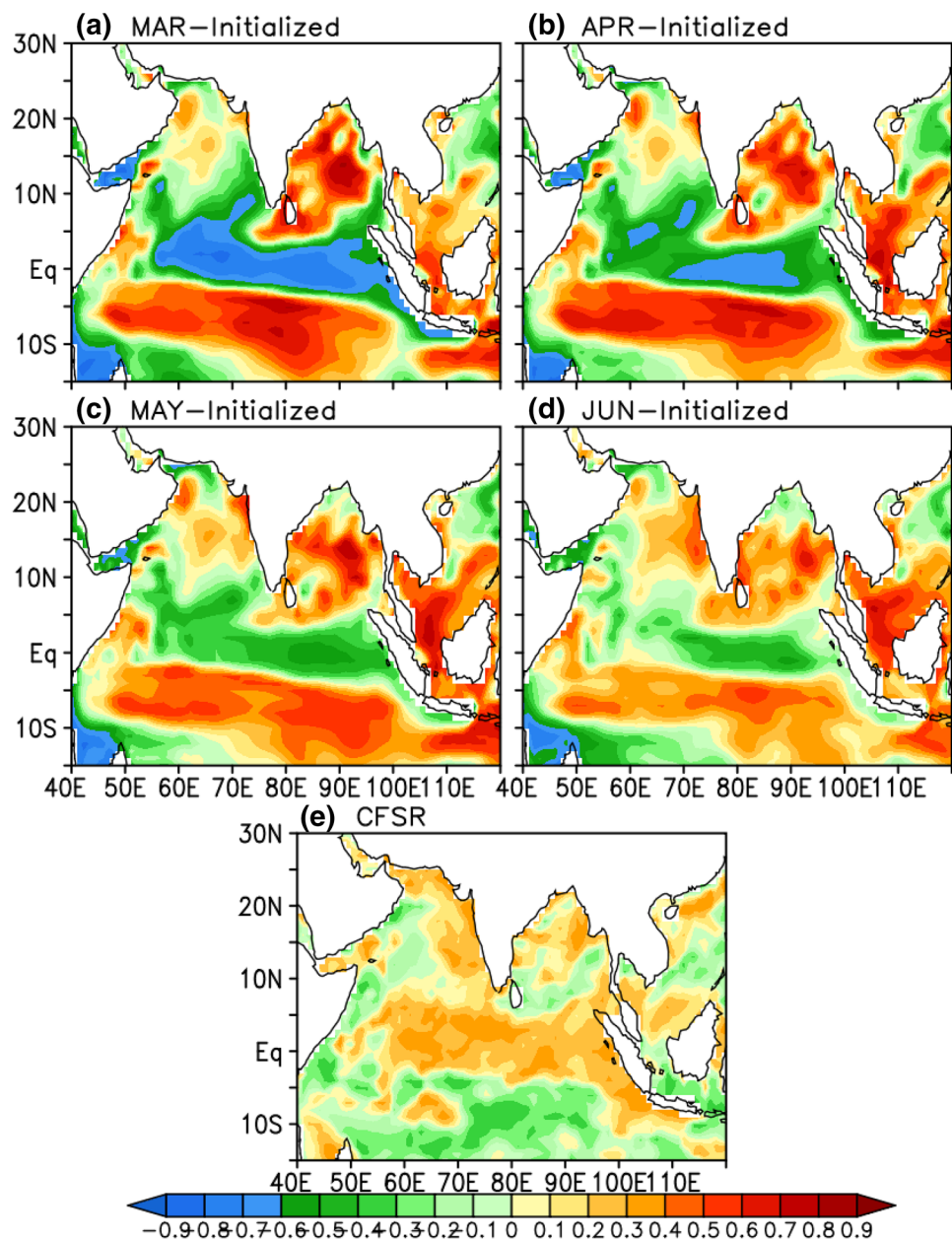
**Fig. 8** Vertical gradient of potential temperature as produced in March- to June-initialized forecasts and CFSR in **a** BOB, **b** AS and **c** southern IO. The Y-axis depicts ocean depth in meters



Murtugudde et al. 2000; Waliser et al. 2003, 2004). In the CFSv2 forecasts, the positive MLD biases in the IO basin stem from the low-level atmospheric wind biases in the western IO that grow with the lead time of the forecasts (Chowdary et al. 2015; Narapusetty et al. 2015). The ENSO-related increase in the anomalous easterlies in the IO basin and the strengthened descending branch of Walker circulation are also driving forces for the MLD biases in the CFSv2 forecasts (Achuthavarier et al. 2012; Jiang et al. 2013). Figure 9 shows the correlation of Niño3 (SST anomaly averaged over 90°W–150°W and 5°S–5°N) with MLDs in July–August averaged forecasts and observations. Compared to observations, the forecasts show an

opposite relationship between Niño3 and MLDs in the AS and IO basins. In northern AS, observations are marked with negative correlations off the coast of the Arabian Peninsula and positive correlations off the west coast of India, whereas, the Mar- to May-initialized forecasts exhibit correlations opposite in sign. However, only the Jun-initialized forecasts have similar correlations in the AS in observations. Over the IO, the forecasts show a tripole zonal structure of Niño3-MLD correlations with positive correlations south of Sri Lanka, negative correlations in the EIO and positive correlations in southeastern IO, whereas the observations show exactly opposite signs for this tripole structure of correlations. Observations

**Fig. 9** Correlation between Niño3 and mixed layer depths in **a** March- **b** April- **c** May- and **d** June-initialized forecasts. The observed correlation is shown in **e**



show a weak negative correlation in the northern BoB followed by a weak positive correlation off the coast of southern India, whereas the Mar- to Apr-initialized forecasts show strong positive correlations throughout the basin and the May- to Jun-initialized forecasts reproduce the correct sign of correlations coherent with observations. These correlations suggest that the MLDs produced by the forecasts in the AS, IO and BoB are excessively influenced by Pacific Ocean SSTs.

Table 3 compares the total number of break days in MAR- to JUN-initialized July and August forecasts with CSFR data in El Niño years. Except for the years 1982 and 1987, the CFSv2 forecasts consistently produce higher number of break days. The increase of break days in ENSO years is coherent with the findings by Dwivedi et al. (2015), which show that the increase in break spells is associated with the ENSO induced large-scale temperature shifts in the troposphere coupled with late onset and early withdrawal of the monsoon. The current study shows that the AS, IO and BoB basins in CFSv2 forecasts are strongly influenced by Pacific SSTs along with systematic delay in monsoon onset. Though the delay in the monsoonal onset is argued to be affected by the northward propagating activities (Zhou and Murtugudde 2014), it is unclear if such a relation exists in CFSv2. It is nonetheless apparent that the wind biases that are stronger in the beginning of the monsoon further lead to feedbacks that actually weaken the moisture transport throughout JJAS (Narapusetty et al. 2015; Ramakrishna et al. 2016; Pathak et al. 2017). Among the Mar- to Jun-initialized forecasts, there are no clear systematic higher break days attributable to a particular initialized month; however, the JUN-initialized forecasts produce lower break days than the Mar- to May-initialized forecasts in four out of the nine ENSO years (i.e., 1986, 1997, 2004 and 2006).

### 4 Conclusions

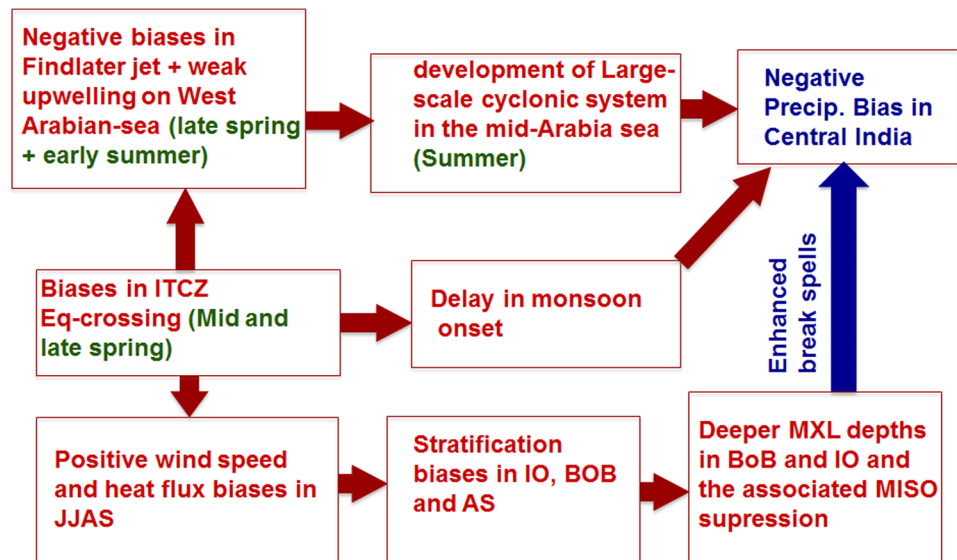
The main goal of this study is to elicit the ocean–atmosphere processes in AS, IO and BoB basins associated with extended break spells and their influence on the dry-land bias during ISMR, particularly in July and August as produced by CFSv2. The CFSv2 hindcasts in the summer months of 1982–2007 at sub-daily and monthly resolutions obtained by initializing in March to June are examined for understanding how the higher number of break events contribute to the precipitation deficits in ISMR. Several systematic biases in CFSv2 forecasts contributing to the dry-land bias are analyzed in this study.

The key features of ISMR’s spatial distribution such as negative correlations of the core monsoon zone with the southern peninsula and the Himalayan foothills, positive correlations along Western Ghats and northwest-southeast tilt of precipitation are missing in the CFSv2 summer forecasts produced by initializing in March to May. However, the Jun-initialized forecasts partially capture these important features suggesting that the spatial distribution of forecasted precipitation over India could be improved. Most of the ensemble forecasts initialized in March to May produce more break days while the concurrent observations show a much lower number in majority of the years. The total as well as intraseasonal component of the precipitation is found to be very weak in all the CFSv2 forecasts except in the JUN-initialized forecasts, which show a promising rendition of strength and variability. The ocean–atmosphere biases that lead to the systematic dry-land bias in CFSv2 forecasts have been extensively studied elsewhere (Narapusetty et al. 2015). In this study, the weaker intraseasonal variability in precipitation is found to be sensitive to the persistent negative vorticity over northern AS in conjunction with biases in the Findlater jet and MLDs in the northern BoB and

**Table 3** Total break days in July–August of ENSO years in Mar- to Jun-initialized forecasts and CSFR

Year	Standardized NINO3 anomaly (CFSR)	Break days					CFSR
		CE’Sv2 forecasts					
		Mar	Apr	May	Jun		
1982	2.03	0	0	0	3	7	
1986	0.45	12	3	21	4	9	
1987	1.08	10	0	4	15	17	
1991	0.53	0	3	0	3	0	
1994	0.51	0	0	4	3	0	
1997	3.06	9	21	29	6	8	
2002	1.05	14	15	21	27	20	
2004	0.55	23	27	19	8	9	
2006	1.05	18	33	11	7	0	

**Fig. 10** Schematic diagram of bias propagation that leads to dry-land biases over central India in CFSv2 forecasts



EIO. The negative vorticity biases in the AS extend over to central India in the Mar- and Apr-initialized forecasts while systematically reduce in May- and Jun-initialized forecasts. The Mar- and Apr-initialized forecasts produce deeper MLDs in July and August in the northern BoB and EIO, which act to suppress the intraseasonal variability and increase the total number of break days, which in turn contribute to the dry-land biases. However, the May- and Jun-initialized forecasts reproduce realistic shoaling of the mixed layer and hence forecast stronger intraseasonal variations. This study reveals that the May- and the Jun-initialized forecasts reproduce the intraseasonal and the total ISMR in July and August reliably by alleviating the ocean–atmosphere coupled biases and the associated feedbacks. There are consistent biases in the vertical structure in the ocean as expected. Candidates for the upper ocean bias include a deficient representation of mixing and errors in freshwater forcing among others (Howden and Murtugudde 2001; Jochum and Potemra 2008; Jochum et al. 2013). Figure 10 synthesizes the pathways of bias propagation that lead to the dry bias over central India. Narapusetty et al. (2015) showed the evolution of ocean–atmospheric biases that lead to the deficit in ISMR in the seasonal forecasts produced by CFSv2. The schematic diagram here depicts the pathways that lead to dry bias over central India by enhancing the number of break days coupled with the delay in the monsoon onset.

The role of ENSO and Atlantic zonal modes (Pottapinjara et al. 2014, 2016) on shoaling the mixed layers in the CFSv2 simulations and forecasts should provide more insights on the potential sources of biases as well as on the ways to improve prediction skill of intraseasonal variability, especially during the non-ENSO years. Such a study is underway and the results will be reported elsewhere.

**Acknowledgements** The authors gratefully acknowledge the financial support given by the Earth System Science Organization, Ministry of Earth Sciences, Government of India (MM/SERP/Univ\_Maryland\_USA/2013/INT-16/002) to conduct this research under Monsoon Mission. The authors also acknowledge Dr. Krishnan, Dr. Rajeevan, Dr. Shukla, Dr. Kinter, and two anonymous reviewers for helpful comments and discussions.

## References

- Abhilash S, Sahai AK, Borah N, Chattopadhyay R, Joseph S, Sharmilla S, De S, Goswami BN, Kumar A (2014) Prediction and monitoring of monsoon intraseasonal oscillations over Indian monsoon region in an ensemble prediction system using CFSv2. *Clim Dyn* 42:2801–2815. <https://doi.org/10.1007/s00382-013-2045-9>
- Achuthavarier D, Krishnamurthy V (2010) Relation between intraseasonal and interannual variability of the south Asian monsoon in the National Centers for Environmental Predictions forecast systems. *J Geophys Res*. <https://doi.org/10.1029/2009JD012865>
- Achuthavarier D, Krishnamurthy V, Kirtman BP, Huang B (2012) Role of Indian Ocean in the ENSO-Indian summer monsoon teleconnection in the NCEP climate forecast system. *J Clim* 25:2490–2508
- Alexander MA, Bladé I, Newman M, Lanzante JR, Lau N-C, Scott JD (2002) The atmospheric bridge: the influence of ENSO teleconnections on air-sea interaction over the global oceans. *J Clim* 15:2205–2231. [https://doi.org/10.1175/1520-0442\(2002\)0152.0.CO;2](https://doi.org/10.1175/1520-0442(2002)0152.0.CO;2)
- Annamalai H, Slingo JM (2001) Active/break cycles: diagnosis of the intraseasonal variability of the Asian summer monsoon. *Clim Dyn* 18:85–102
- Ashfaq M, Rastogi D, Mei R, Touma D, Leung RL (2016) Sources of errors in the simulation of south Asian summer monsoon in CMIP5 GCMs. *Clim Dyn Online*. <https://doi.org/10.1007/s00382-016-3337-7>
- Borah N, Sahai AK, Chattopadhyay R, Joseph S, Abhilash S, Goswami BN (2013) A self-organizing map based ensemble forecast system for extended range prediction of active/break cycles of Indian summer monsoon. *J Geophys Res Atmos* 118:1–13. <https://doi.org/10.1002/jgrd.50688>

- Chattopadhyay R, Rao SA, Sabeerali CT, George G, Rao DN, Dhakate A, Salunke K (2015) Large-scale teleconnection patterns of Indian summer monsoon as revealed by CFSv2 retrospective seasonal forecast runs. *Int J Climatol*. <https://doi.org/10.1002/joc.4556>
- Chaudhari HS, Pokhrel S, Saha SK, Dhakate A, Yadav RK, Salunke K, Mahapatra S, Sabeerali CT, Rao SA (2012) Model biases in long coupled runs of NCEP CFS in the context of Indian summer monsoon. *Inter J Climatol* 33:1059–1063. <https://doi.org/10.1002/joc.3489>
- Chen X, Ling J, Li C (2016) Evolution of Madden–Julian Oscillation in two types of El Niño. *J Clim* 29(5):1919–1934
- Chowdary JS, Parekh A, Sayantani O, Gnanaseelan C (2015) Role of upper ocean processes in the seasonal SST evolution over tropical Indian Ocean in climate forecasting system. *Clim Dyn*. <https://doi.org/10.1007/s00382-015-2478-4>
- DelSole T, Shukla J (2012) Climate models produce skillful predictions of Indian summer monsoon rainfall. *Geophys Res Lett* 39:L09703. <https://doi.org/10.1029/2012GL051279>
- Drushka K, Sprintall J, Gille S, Wijffels S (2012) In situ observations of Madden–Julian Oscillation mixed layer dynamics in the Indian and western Pacific Oceans. *J Clim* 25(7):2306–2328
- Drushka K, Sprintall J, Gille ST (2014) Subseasonal variations in salinity and barrier-layer thickness in the eastern equatorial Indian Ocean. *J Geophys Res* 119:805–823
- Dwivedi S, Goswami BN, Kucharski F (2015) Unraveling the missing link of ENSO control over the Indian monsoon rainfall. *Geophys Res Lett* 42:8201–8207. <https://doi.org/10.1002/2015GL065909>
- Feng J, Liu P, Chen W, Wang XC (2015) Contrasting Madden–Julian oscillation activity during various stages of EP and CP El Niños. *Atmos Sci Lett* 16:32–37
- Gadgil S, Joseph PV (2003) On breaks of the Indian monsoon. *Proc Indian Acad Sci (Earth Planet Sci)* 112:529–558
- Gadgil S, Rupa Kumar K (2006) The Asian monsoon—agriculture and economy. In: Wang B (ed.) *The Asian Monsoon*, vol 5. Springer Praxis, Honolulu, pp 651–683
- Goswami BN, Ajaya Mohan RS (2001) Intraseasonal oscillations and interannual variability of the Indian summer monsoon. *J Clim* 14:1180–1198
- Goswami BN, Xavier P (2005) ENSO control on the Asian monsoon through the length of the rainy season. *Geophys Res Lett* 32:1–4. <https://doi.org/10.1029/2005GL023216>
- Goswami BB, Deshpande M, Mukhopadhyay P, Saha SK, Rao SA, Murthugudde R, Goswami BN (2014) Simulation of Indian summer monsoon intraseasonal oscillation variability in NCEP CFSv2 and its role on systematic bias. *Clim Dyn* 43:2725–2745. <https://doi.org/10.1007/s00382-014-2089-5>
- Howden SD, Murtugudde R (2001) Effects of river inputs into the Bay of Bengal. *J Geophys Res* 106:19825–19843
- Jiang X, Yang S, Li J, Li Y, Hu H, Lian Y (2013) Variability of the Indian Ocean SST and its possible impact on summer western North Pacific anticyclone in the NCEP climate forecast system. *Clim Dyn* 41:2199–2212
- Jochum M, Potemra J (2008) Sensitivity of tropical rainfall to Banda Sea diffusivity in the community climate system model. *J Clim* 21:6445–6454
- Jochum MB, Briegleb P, Danabasoglu G, Large WG, Norton NJ, Jayne SR, Alford MH, Bryan FO (2013) The impact of oceanic near-inertial waves on climate. *J Clim* 26:2833–2844. <https://doi.org/10.1175/JCLI-D-12-00181.1>
- Keerthi MG, Lengaigne M, Vialard J, de Boyer Montégut C, Muraleedharan PM (2013) Interannual variability of the Tropical Indian Ocean mixed layer depth. *Clim Dyn* 40:743–759
- Klein SA, Soden BJ, Lau N-C (1999) Remote sea surface temperature variations during ENSO: evidence for a tropical atmospheric bridge. *J Clim* 12:917–932
- Krishna Kumar K, Rupa Kumar K, Ashrit R, Deshpande NR, Hansen JW (2004) Climate impacts on Indian agriculture. *Int J Climatol* 24:1375–1393
- Krishnamurthy V (2016) Intraseasonal oscillations in East Asian and South Asian monsoons. *Clim Dyn*. <https://doi.org/10.1007/s00382-016-3466-z>
- Krishnamurthy V (2017) Predictability of CFSv2 in the tropical Indo-Pacific region, at daily and subseasonal time scales. *Clim Dyn*. <https://doi.org/10.1007/s00382-017-3855-y>
- Krishnamurthy V, Shukla J (2000) Intraseasonal and interannual variability of rainfall over India. *J Clim* 13:4366–4377
- Krishnamurthy V, Shukla J (2008) Seasonal persistence and propagation of intraseasonal patterns over the Indian monsoon region. *Clim Dyn* 30:353–369
- Krishnamurti TN, Ardanuy P (1980) The 10–20 day westward propagating mode and breaks in the monsoon. *Tellus* 32:15–26
- Lau N-C, Nath MJ (2000) Impact of ENSO on the variability of the Asian–Australian monsoons as simulated in GCM experiments. *J Clim* 13:4287–4309
- Lau N-C, Nath MJ (2003) Atmosphere–ocean variations in the Indo Pacific sector during ENSO episodes. *J Clim* 16:3–20
- Lee JY, Wang B, Kang IS, Shukla J, Kumar A, Kug JS, Schemm JKE, Luo JJ, Yamagata T, Fu X, Alves O, Stern B, Rosati T, Park-Show CK (2010) How are seasonal prediction skills related to models’ performance on mean state and annual cycle? *Clim Dyn* 35(2):267–283. <https://doi.org/10.1007/s00382-010-0857-4>
- Lee Drbohlav H, Krishnamurthy V (2010) Spatial structure, forecast errors, and predictability of the South Asian monsoon in CFS monthly retrospective forecasts. *J Clim* 23:4750–4769. <https://doi.org/10.1175/2010JCLI2356.1>
- Li Y, Han W, Wang W, Ravichandran M (2016) Intraseasonal variability of SST and precipitation in the Arabian Sea during Indian summer monsoon: Impact of the ocean mixed layer depth. *J Clim* 29:7889–7910
- Li Y, Han W, Wang W, Ravichandran M, Lee T, Shinoda T (2017) Bay of Bengal salinity stratification and Indian summer monsoon intraseasonal oscillation: 2. Impact on SST and convection. *J Geophys Res Oceans*. <https://doi.org/10.1002/2017JC012692>
- Liu F, Zhou L, Ling J, Fu X, Huang G (2016) Relationship between SST anomalies and the intensity of intraseasonal variability. *Theor Appl Climatol*. <https://doi.org/10.1007/s00704-015-1458-2>
- Meehl GA, Arblaster JM, Caron JM, Annamalai H, Jochum M, Chakraborty A, Murtugudde R (2012) Monsoon regimes and processes in CCSM4. Part I: The Asian–Australian monsoon. *J Clim* 25:2583–2608. <https://doi.org/10.1175/JCLI-D-11-00184.1>
- Murtugudde R, Busalacchi AJ (1999) Interannual variability of the dynamics and thermodynamics of the tropical Indian Ocean. *J Clim* 12:2300–2326. [https://doi.org/10.1175/1520-0442\(1999\)012<2300:IVOTDA>2.0.CO;2](https://doi.org/10.1175/1520-0442(1999)012<2300:IVOTDA>2.0.CO;2)
- Murtugudde R, McCreary JP, Busalacchi AJ (2000) Oceanic processes associated with anomalous events in the Indian Ocean with relevance to 1997–1998. *J Geophys Res* 105:3295–3306
- Narapusetty B, DelSole T, Tippett MK (2009) Optimal estimation of the climatological mean. *J Clim* 22:4845–4859. <https://doi.org/10.1175/2009JCLI2944.1>
- Narapusetty B, Murtugudde R, Wang H, Kumar A (2015) Ocean–atmosphere processes driving Indian summer monsoon biases in CFSv2 hindcasts. *Clim Dyn* 47:1417–1433. <https://doi.org/10.1007/s00382-015-2910-9>
- Pathak A, Ghosh S, Kumar P, Murtugudde R (2017) Role of oceanic and terrestrial atmospheric moisture sources in intraseasonal variability of Indian summer monsoon rainfall. *Sci Rep* 7:12729. <https://doi.org/10.1038/s41598-017-13115-7>
- Pokhrel S, Dhakate A, Chaudhari HS, Saha SK (2013) Status of NCEP CFS vis-a-vis IPCC AR4 models for the simulation of Indian summer monsoon. *Theor Appl Climatol* 111:65–78

- Pokhrel S, Saha SK, Dhakate A, Rahman H, Chaudhari HS, Salunke K, Hazra A, Sujith K, Sikka DR (2016) Seasonal prediction of Indian summer monsoon rainfall in NCEP CFSv2: forecast and predictability error. *Clim Dyn* 46:2305–2326
- Pottapinjara V, Girishkumar MS, Ravichandran M, Murtugudde R (2014) Influence of the Atlantic zonal mode on monsoon depressions in the Bay of Bengal during boreal summer. *J Geophys Res Atmos* 19(11):6456–6469. <https://doi.org/10.1002/2014JD021494>
- Pottapinjara V, Girishkumar MS, Ravichandran M, Murtugudde R (2016) Relation between the upper ocean heat content in the equatorial Atlantic during boreal spring and the Indian monsoon rainfall during June–September. *Int J Climatol* 36:2469–2480. <https://doi.org/10.1002/joc.4506>
- Prasanna V (2014) Impact of monsoon rainfall on the total food grain yield over India. *J Earth Syst Sci* 123(5):1129–1145
- Rajeevan M, Gadgil S, Bhatte J (2010) Active and break spells of the Indian summer monsoon. *J Earth Syst Sci* 119(3):229–247
- Ramakrishna SSVS., Brahmananda Rao V, Srinivasa Rao BR, Hari Prasad D, Nanaji Rao N, Panda R (2016) A study of 2014 record drought in India with CFSv2 model: role of water vapor transport. *Clim Dyn* 49:297–312. <https://doi.org/10.1007/s00382-016-3343-9>
- Ramamurthy K (1969) Some aspects of the “Break” in the Indian Southwest Monsoon during July and August, *Forecasting Manual No.IV-18.3*. India Meteorological Department, Pune, India, pp 1–57
- Roxy M, Tanimoto Y, Preethi B, Terray P, Krishnan R (2013) Intraseasonal SST-precipitation relationship and its spatial variability over the tropical summer monsoon region. *Clim Dyn* 41(1):45–61
- Saha S, Moorthi S, Pan H-L, Wu X, Wang J, Nadiga S, Tripp P, Kistler R, Woollen J, Behringer D, Liu H, Stokes D, Grumbine R, Gayno G, Wang J, Hou Y-T, Chuang H-Y, Juang HMH, Sela J, Iredell M, Treadon R, Kleist D, Delst PV, Keyser D, Derber J, Ek M, Meng J, Wei H, Yang R, Lord S, Van Den Dool H, Kumar A, Wang W, Long C, Chelliah M, Xue Y, Huang B, Schemm JK, Ebisuzaki W, Lin R, Xie P, Chen M, Zhou S, Higgins W, Zou C-Z, Liu Q, Chen Y, Han Y, Cucurull L, Reynolds RW, Rutledge G, Goldberg M (2010) The NCEP climate forecast system reanalysis. *Bull Am Meteorol Soc* 91:1015–1057. <https://doi.org/10.1175/2010BAMS3001.1>
- Saha S, Moorthi S, Wu X, Wang J, Nadiga S, Tripp P, Behringer D, Hou Y, Chuang H, Iredell M, Ek M, Meng J, Rongqian Yang R, Mendez MP, van den Dool H, Zhang Q, Wang W, Chen M, Becker E (2014) The NCEP climate forecast system version 2. *J Clim* 27:2185–2208. <https://doi.org/10.1175/JCLI-D-12-00823.1>
- Sahai AK, Sharmila S, Abhilash S, Chattopadhyay R, Borah N, Krishna RPM, Joseph S, Roxy M, De S, Pattnaik S, Pillai PA (2013) Simulation and extended range prediction of monsoon intraseasonal oscillations in NCEP CFS/GFS version 2 framework. *Curr Sci* 104(10):1394–1408
- Sikka DR, Gadgil S (1980) On the maximum cloud zone and the ITCZ over Indian, longitudes during the southwest monsoon. *Mon Wea Rev* 108:1840–1853
- Sperber KR, Annamalai H, Kang IS, Kitoh A, Moise A, Turner A, Wang B, Zhou T (2013) The Asian summer monsoon: an inter-comparison of CMIP5 vs. CMIP3 simulations of the late 20th century. *Clim Dyn*. <https://doi.org/10.1007/s00382-012-1607-6>
- Vinayachandran PN, Neema CP, Mathew S, Remya R (2012) Mechanisms of summer intraseasonal sea surface temperature oscillations in the Bay of Bengal. *J Geophys Res* 117:C01005. <https://doi.org/10.1029/2011JC007433>
- Waliser DE, Murtugudde R, Lucas LE (2003) Indo-Pacific Ocean response to atmospheric intraseasonal variability: 1. Austral summer and the Madden–Julian oscillation. *J Geophys Res* 108(C5):3160. <https://doi.org/10.1029/2002JC001620>
- Waliser DE, Murtugudde R, Lucas LE (2004) Indo-Pacific Ocean response to atmospheric intraseasonal variability: 2. Boreal summer and the intraseasonal oscillation. *J Geophys Res* 109:C03030. <https://doi.org/10.1029/2003JC002002>
- Wang B, Ding Q, Joseph PV (2009) Objective definition of the Indian summer monsoon onset. *J Clim* 22:3303–3316. <https://doi.org/10.1175/2008JCLI2675.1>
- Wu R, Cao X (2017) Relationship of boreal summer 10–20-day and 30–60-day intraseasonal oscillation intensity over the tropical western North Pacific to tropical Indo-Pacific SST. *Clim Dyn* 48:3529–3546. <https://doi.org/10.1007/s00382-016-3282-5>
- Xi J, Zhou L, Murtugudde R, Jiang L (2015) Impacts of intraseasonal sst anomalies on precipitation during Indian summer monsoon. *J Clim* 28:4561–4575
- Yasunari T (1980) A quasi-stationary appearance of 30–40 day period in the cloudiness fluctuations during the summer monsoon over India. *J Meteorol Soc Jpn* 58:225–229
- Yasunari T (1981) Structure of an Indian summer monsoon system with around 40-day period. *J Meteorol Soc Jpn* 59:336–354
- Yatagai A, Kamiguchi K, Arakawa O, Hamada A, Yasutomi N, Kitoh A (2012) APHRODITE: constructing a long-term daily gridded precipitation dataset for Asia based on a dense network of rain gauges. *Bull Am Meteorol Soc* 93:1401–1415. <https://doi.org/10.1175/BAMS-D-11-00122.1>. <https://doi.org/10.1016/j.dynatmoce.2009.12.003>
- Zhou L, Murtugudde R (2014) Impact of northward propagating intraseasonal variability on the onset of Indian summer monsoon. *J Clim* 27:126–139. <https://doi.org/10.1175/JCLI-D-13-00214.1>
- Zhou L, Murtugudde R, Chen D, Tang Y (2016) A Central Indian Ocean Mode and Heavy Precipitation during the Indian Summer Monsoon. *J Clim* 30:2055–2067. <https://doi.org/10.1175/JCLI-D-16-0347.1>
- Zhou L, Murtugudde R, Chen D, Tang Y (2017) Seasonal and inter-annual variabilities of the central Indian Ocean mode. *J Clim* 30:6505–6520. <https://doi.org/10.1175/JCLI-D-16-0616.1>